Journal of The Electrochemical Society, **151** (10) C674-C679 (2004)
0013-4651/2004/151(10)/C674/6/$7.00 © The Electrochemical Society, Inc.

Macro Internal Structures of Porous Ni-P Films Electrodeposited under Galvanostatic Conditions

M. Saitou*,z and Y. Okudaira

Department of Mechanical Systems Engineering, University of the Ryukyus, Okinawa, 098-0213 Japan

Using a laser profile microscope, we have investigated the internal structures of porous Ni-P electrodeposits grown under fixed current densities to find some properties that characterize the structure of the electrodeposits. The statistical analysis of the digitized microscope images reveals that the porous Ni-P deposits distribute according to a Poisson distribution and have values of the fractal dimension and scaling exponent different from those of the diffusion-limited aggregation model. Another result is that the number of ions at the cathode electrode oscillates at a fundamental frequency, which fact is interpreted by the presence of an oscillatory solution of the electrochemical rate equations in the Ni-P-H system using linearized perturbation equations.
 [DOI: 10.1149/1.1793193]

Manuscript submitted July 18, 2003; revised manuscript received March 29, 2004. Available electronically September 27, 2004.

Various morphologies in electrodeposition named dense structures, elongated finger arrays, forests of trees, and dendrites have been recognized experimentally and have also received much theoretical interest.[1] The dynamics of pattern formation are often interpreted on the basis of a diffusion-limited aggregation (DLA),[2] that gives the fractal dimension $d_f(d,db)$ on the d_b-dimensional surface of substrates in the d-dimensional space.[3] In addition, scaling properties that describe the structures of electrodeposits have been studied quantitatively using power-law treatments.

These experimental investigations into the morphologies have been made mainly for single-element electrodeposits in a confined thin cell. For the co-electrodeposition of two and more ion elements, the morphological growth phenomenon becomes more complicated, and other types of morphological transitions and morphologies are observed. For example, the presence of spherical pores in nickel electrodeposits[4] was reported and suggests that the pores in the nickel films become spherical owing to the stable electrochemical reaction $2H^+ + 2e \rightarrow H_2$.

Unfortunately, there have been very few studies on macro internal structures and their characterizations of porous Ni-P electrodeposits. Ni-P alloys generally serve as substrates for magnetic materials in thin-layer magnetic storage devices.[5] In this study, nickel, phosphorus, and hydrogen atoms are deposited at cathode electrodes in typical electrolytes under fixed current densities. The pores in the Ni-P electrodeposits appear to be string-like aggregates different from those in pure nickel electrodeposits. The porous structures in the Ni-P electrodeposits are analyzed using digitized microscope images of the Ni-P electrodeposits.

This paper aims at presenting the characteristic properties of the porous Ni-P structures in terms of periodic structures, scaling properties, and oscillatory behaviors in deposition. In particular, the oscillatory deposition behavior is analyzed on the basis of analysis of linearized perturbation equations in electrochemical reactions of the Ni-P-H system.

Experimental

The experimental procedure for Ni-P electrodeposition at fixed current densities was as follows: copper and carbon plates 1 cm wide and 3 cm long were prepared for cathode and anode electrodes. The mirror-like copper and carbon plates were cleaned by a wet process and placed parallel in a still bath containing (g/L): nickel sulfate, 148; nickel chloride, 45; nickel carbonate basic, 32; phosphorous acid, 20; and phosphoric acid, 35. The bath was maintained at a temperature of 323 K. A fixed current density ranging from 10 to 40 mA/cm^2 was applied during electrodeposition. The phosphorus concentrations in the electrodeposits were measured with electron probe microanalysis (EPMA). The Ni-P electrodeposit on the copper plate was embedded in a polyester resin. After the resin hardened, the samples were polished to observe with a laser profile microscope that has an accuracy of the order of 0.23 μm. The digitized cross-sectional microscope images comprise 480 × 752 pixels.

Results and Discussion

Scaling and self-similarity are important concepts in modern statistical physics, especially in phase transitions. Scaling is often described by simple power laws consisting of the exponents, irrespective of experimental details and specific experimental systems. Electrodeposition, which is a kind of phase transition, exhibits scaling and self-similar properties insensitive to experimental details such as electrodeposition in the electrolyte under quiescent or stirring conditions. This is one reason why scaling treatments are chosen to analyze the experimental results.

Scaling properties.—Figure 1 shows the cross-sectional images of the Ni-P electrodeposits observed with the laser profile microscope. The dark regions are empty, and the bright regions in Fig. 1c and d seem to be string-like structures. The porous structures appear to have no spherical shape, which is different from those observed in pure nickel electrodeposits.[4] Generally, the nucleation rate of electrodeposits increases by using pulse currents instead of fixed currents. If that is true for the gas formation of hydrogen, we may control the nucleation rate of the hydrogen gas bubbles and may solve a question of why the porosity in this experiment has no semiglobular or no semioval shape. These porous images of the Ni-P electrodeposits do not depend on planes polished in directions parallel to the growth direction. The Ni-P electrodeposit grown at a current density of 10 mA/cm^2 has a dense structure, which changes into a porous structure at a current density of 20 mA/cm^2. The structure in Fig. 1b shows that the porous Ni-P deposits are grown at the initial stage and after that, the dense Ni-P appears, which suggests that the growth mechanism is unstable even under the fixed current density. In a previous paper,[6] we report that under a fixed current density and the high initial ion concentrations of $[Ni^{2+}]$ and $[H_3PO^{3-}]$, even if hydrogen evolves, the concentration ratio of P to Ni may remain unchanged. Hence, in Fig. 1b, the P concentration in the dense portion may be similar to that in the porous portion.

To measure the abrupt transition quantitatively, the porosities defined by the ratio of the number of pixels in the dark regions to the number of the total pixels of the image are calculated from the cross-sectional images of the Ni-P electrodeposits. The phosphorus concentration investigated with EPMA[6] and the porosity in the Ni-P electrodeposits are plotted in Fig. 2. It can be seen that the porosity increases with a decrease in the phosphorus concentration. The current passes through the electrolyte, reducing nickel, phosphorus, and hydrogen ions at the cathodes. The mechanism of phosphorus incorporation into nickel electrodeposits has been reported, which is due to the phosphine gas PH_3 evolved at the cathode electrodes.[7] Under the fixed current density, the decrease in the phosphorus concentra-

* Electrochemical Society Active Member.
z E-mail: saitou@tec.u-ryukyu.ac.jp

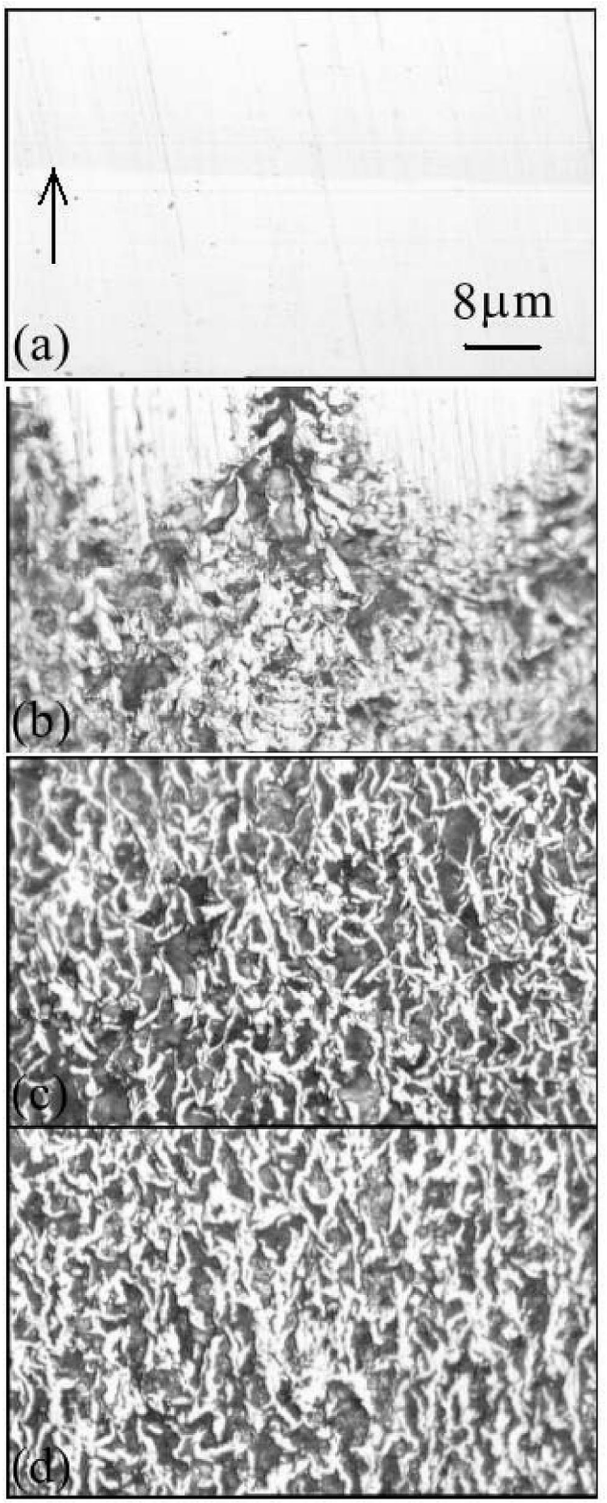

Figure 1. Cross-sectional microscope images of the Ni-P electrodeposits for a current density (mA/cm^2): (a) 10, (b) 20, (c) 30, and (d) 40. The dark regions are empty. The string-like structures in the bright regions in b-d are Ni-P alloys. The arrow in a shows a growth direction of the Ni-P electrodeposits on the copper substrate.

tion in the Ni-P electrodeposits implies an increase in the hydrogen gas evolved at the cathode electrodes. Hence, the hydrogen gas

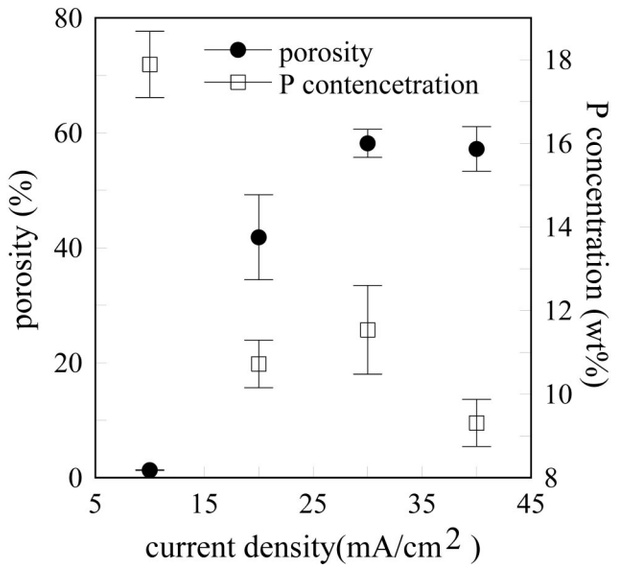

Figure 2. Average porosities and phosphorus concentration of the Ni-P films electrodeposited for the current densities in a range from 10 to 40 mA/cm^2. These porosities are calculated from the binary image of the cross-sectional microscope images. The phosphorus concentrations in the electrodeposits are measured with EPMA.

evolved at the cathodes plays a main role in the formation of the porous structures in the Ni-P electrodeposits.

Do the string-like Ni-P images in Fig. 1b-d have some periodical and symmetrical structure? Using a fast Fourier transform (FFT) technique, Fig. 3 shows a typical power spectrum image of Fig. 1c, which depicts a hollow pattern but not some straight lines and dots. Hence, it is concluded that no periodical structure of the Ni-P deposits can be recognized.

We examine scaling properties of the porous Ni-P electrodeposits. All the cross-sectional microphotographs digitized with a resolution of 480 × 752 pixels are transformed into binary images. The root-mean-square (rms) thickness and the number of pixels that lie with a thickness of h and under are defined by

$$T(h) = \langle (x_i - \langle x_i \rangle)^2 \rangle^{1/2} \quad [1]$$

$$N(h) = \sum_{x_i \leq h} \rho(x_i) \quad [2]$$

that is defined as

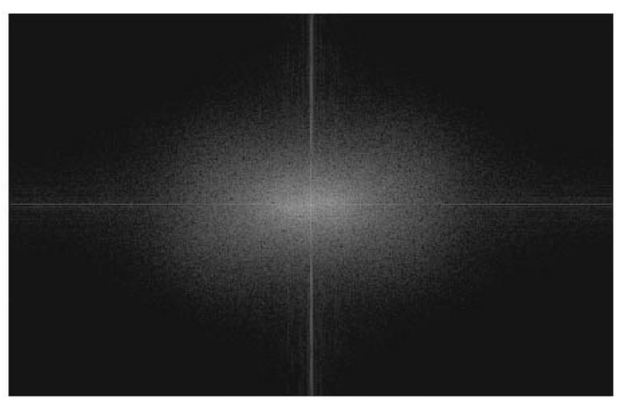

Figure 3. Typical power spectrum image in frequency space into which the original image, Fig. 1c, is transformed using an FFT technique.

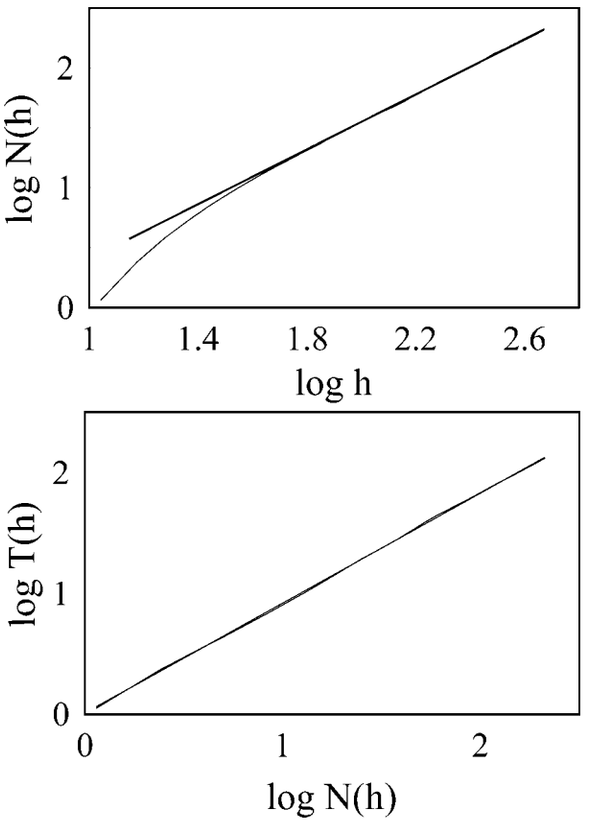

Figure 4. Typical log-log plots of $N(h)$ *vs.* h and $T(h)$ *vs.* $N(h)$. The slopes of the straight lines best fitted to data give the exponents $\alpha = 1.15$ and $\beta = 0.91$ defined as $N(h) \sim h^{\alpha}$ and $T(h) \sim N(h)^{\beta}$.

$$\rho(x_i) = \begin{cases} 1 & \text{if a bright pixel exists at } x_i \\ 0 & \text{if a dark pixel exists at } x_i \end{cases} \quad [3]$$

where $\langle \cdots \rangle$ indicates an average over the number of pixels that exist under a thickness of h, and x_i is the thickness of the pixel i. Equation 2 represents the number of accumulative pixels that lie under a thickness of h that changes in a range of 0 to 479 in units of pixels.

Figure 4 shows that $N(h)$ and $T(h)$ increase as a power of h and $N(h)$, respectively

$$N(h) \propto h^{\alpha} \quad [4]$$

$$T(h) \propto N(h)^{\beta} \quad [5]$$

The values of α and β in Fig. 4 are estimated at 1.15 and 0.910, which yield $\alpha\beta = 1.05$.

Figure 5 shows that when the exponent α increases with the current density, reversely the exponent β decreases. Consequently, we find that

$$\alpha\beta = 1.05 \pm 0.02 \quad [6]$$

which leads to $T(h) \propto h$ in terms of the number of accumulative pixels. It goes without saying that $\langle x_i \rangle \sim h$, which implies that the distribution of the accumulated pixels is determined only by h. In a stochastic process,[8] the mean value m and standard deviation σ are defined by

$$m = \sum x_j P_j \quad [7]$$

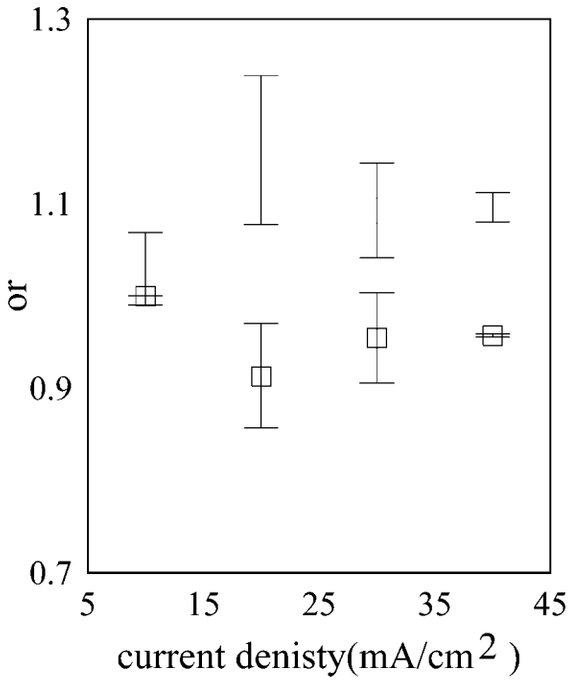

Figure 5. Illustration of the exponents α and β for the different current densities.

$$\sigma^2 = \sum (x_j - \langle x_j \rangle)^2 P_j \quad [8]$$

where P_j is a probability density function. However, the mean and standard deviation values of the accumulative pixels in this study become $m \sim h$ and $\sigma^2 \sim h^2$ from the preceding results. These expectation values associated with h are obtained only if P_j is a type of the following power distribution

$$P_j = \frac{1}{h} \exp\left(-\frac{x_j}{h}\right) \quad [9]$$

which gives a probability distribution of pixels to be found at the x_jth site after a pixel is found at the x_ith site ($x_j > x_i$). The power distribution implies that the Ni-P deposits distribute according to the Poisson distribution.[8] Hence, in Ni-P electrodeposition, the ion particles arriving at the cathode obey the Poisson process. More detailed studies such as numerical simulations based on the Poisson process may be needed to be compared with the porous structure in this study.

Fractal dimension.—We investigate a fractal dimension $d_f(d,d_b)$ of the porous Ni-P electrodeposits that grow on the d_b-dimensional surface in the d-dimensional space. An rms thickness[9] in units of pixels, which is different from Eq. 1, is defined as

$$T_s(h) = \langle x_i^2 \rangle^{1/2} \quad [10]$$

which is measured from the substrates. As reported before,[3] $T_s(h)$ increases as a power of $N(h)$

$$T_s(h) \propto N(h)^{v} \quad [11]$$

The fractal dimension $d_f(d,db)$ is defined by

$$d_f(d,d_b) = d_f(d) - d_b \quad [12]$$

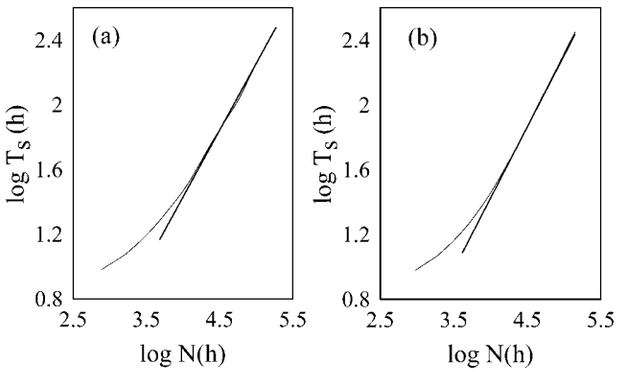

Figure 6. Dependence of the rms thickness $T_s(h)$ on the number of pixels $N(h)$. The straight lines give the slopes best fitted to the data: (a) the current density 20 mA/cm^2, $\nu = 0.91$; (b) the current density 40 mA/cm^2, $\nu = 0.90$.

where $d_f(d)$ is the fractal dimension in the d-dimensional space. The term $d_f(d, db)$ in Eq. 12 indicates the fractal dimension of deposits grown under boundary conditions such as substrates.

Figure 6 shows that the rms $T_s(h)$ increases as a power of $N(h)$ as in the case of the DLA model. For computer simulations of two-dimensional growth on a one-dimensional surface on the basis of the DLA model,[8] $\nu = 1.30$ has been reported. The experiment of zinc-metal trees electrodeposited on a line electrode[3] gave a larger value of $\nu = 1.43$ and $d_f(2) = 1.67$. For the Ni-P electrodeposits as shown in Fig. 6, the values of ν about 0.9 are much less than those in the DLA model. This indicates that, contrary to the growth process in the DLA model, first, the density of the Ni-P electrodeposit does not decrease with the deposition time, and second the ions arriving at the cathode in this experiment are not affected by local effects such as the shadowing generated by the branches of the deposits. Hence, the ions deposited at the cathode have a diffusion length larger than the DLA deposits.

Using a box counting method, the fractal dimension $d_f(d)$ is calculated

$$N_s \propto l^{-d_f(d)} \qquad [13]$$

where N_s is the number of bright pixels that are included in an area of 1×1. The bright pixels correspond to the Ni-P deposits. Figure 7a shows a typical binary image into which the string-like image is transformed. The absolute value of the slope in Fig. 7b is 1.89, which is greater than the value of 1.67 in the DLA model. This also implies that in Ni-P electrodeposition local effects such as shadowing can be negligible and the ions arriving at the cathode can diffuse in contrast to the DLA model.

Oscillatory behavior in electrodeposition.—Next, let us examine how the number of pixels that lie at a thickness of h changes. The number of pixels at a thickness of h is defined as

$$n(h) = \sum_{x_i=h} \rho(x_i) \qquad [14]$$

Figure 8a shows that the number of pixels oscillates with thickness. Figure 8b is a Fourier transformation of $n(h)$, where $P(f)$ is a Fourier transform of $n(h)$ and f is the frequency. The power spectrum indicates that a fundamental frequency f_0 exists. This suggests that even under the fixed total current applied for the reduction of Ni, P, and H ions, their reaction rates may give rise to oscillatory behavior owing to instability in the electrochemical reactions in the Ni-P-H system. Figure 9 shows a typical plot of the cell voltage between the anode and cathode electrode *vs.* the deposition time. For a current density of 15 mA/cm^2 at which the Ni-P film has the dense

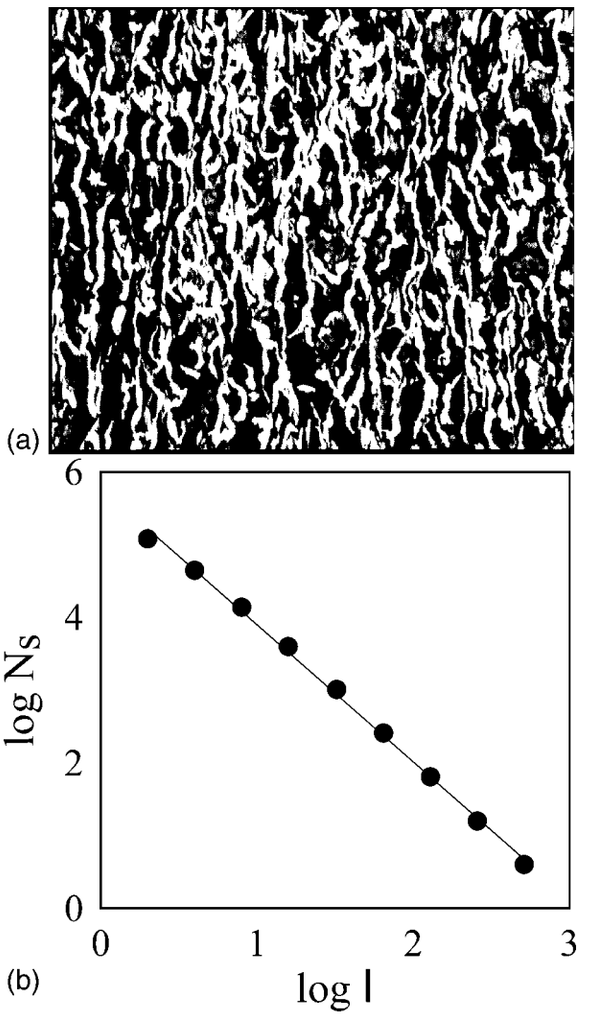

Figure 7. Determination of the fractal dimension $d_f(d)$ using a box counting method: (a) a typical binary image of the porous Ni-P electrodeposit; (b) a log-log plot of N_s *vs.* 1. The straight line best fitted to the data yields $d_f(2) = 1.89$.

structure, the cell voltage asymptotically decreases with time. For 25 mA/cm^2, at which the Ni-P film has a porous structure, the cell voltage changes unstably and oscillates during deposition. The unstable cell voltage after 2500 s in Fig. 9 corresponds to the phase transition from the porous structure to the dense structure as shown in Fig. 1b.

Therefore, we first examine whether or not a condition for the oscillatory deposition in the Ni-P films exists using perturbation equations of the electrochemical reactions. The electrochemical reactions that take place in Ni-P electrodeposition are as follows[7,10]

$$Ni^{2+} + 2e \xrightarrow{k_1} Ni \qquad [15a]$$

$$2H^+ + 2e \xrightarrow{k_2} H_2 \qquad [15b]$$

$$H_2PO_3^- + 2H^+ + 2e \xrightarrow{k_3} H_2PO_2^- + H_2O \qquad [15c]$$

$$H_2PO_3^- + 5H^+ + 4e \xrightarrow{k_4} PH_3 + 2H_2O \qquad [15d]$$

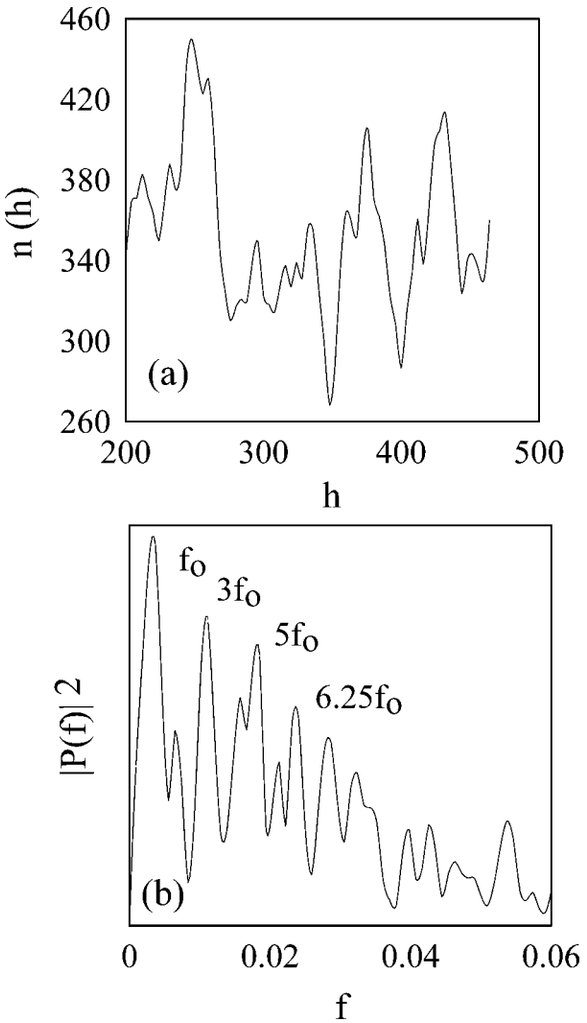

Figure 8. Oscillatory behaviors of $n(h)$ in the porous Ni-P deposits grown at a current density of 40 mA/cm^2: (a) a typical plot of $n(h)$ *vs.* h; (b) power spectrum of $n(h)$ transformed into Fourier space.

$$2PH_3 + 3Ni^{2+} \xrightarrow{k_5} 2P + 3Ni + 6e \quad [15e]$$

$$P + 3H_2O + 3e \xrightarrow{k_6} PH_3 + 3OH^- \quad [15f]$$

$$PH_3 + H_2O \xrightarrow{k_7} PH_4^+ + OH^- \quad [15g]$$

where k_i is the rate constant. Equation 15g[11] represents that phosphine dissolves in water and dissolved phosphine reacts with hydrogen ions to form the phosphonium ion, PH_4^+. The phosphorus element is incorporated into the electrodeposits through the process of the evolution of phosphine gas, which has solubility in the acid solution, as shown in Eq. 15g. Equation 15f acts as a feedback of the phosphine gas that may cause oscillatory chemical reactions. The rate equations are promptly derived

$$\frac{d[PH_3]}{dt} = k_4[H_2PO_2^-][H^+]^5 - 2k_5[PH_3]^2[N^{2+}]^3 + k_6[P] - k_7[PH_3] \quad [16]$$

$$\frac{d[P]}{dt} = 2k_5[PH_3]^2[Ni^{2+}]^3 - k_6[P] \quad [17]$$

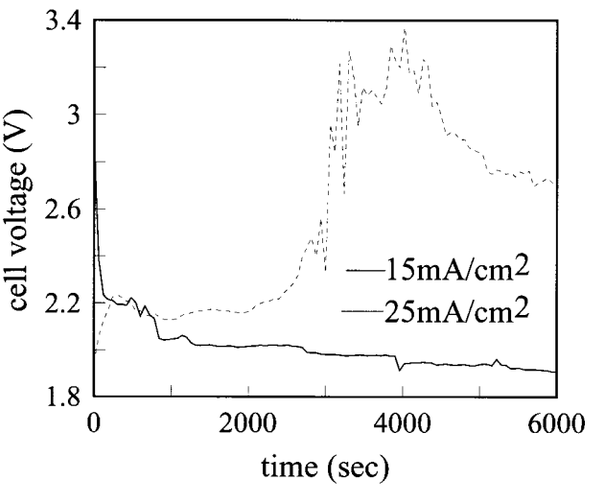

Figure 9. Typical plots of the cell voltage between the anode and cathode electrode *vs.* the deposition time for two different current densities.

$$\frac{d[H^+]}{dt} = -2k_2[H^+]^2 - 2k_3[H^+]^2[H_2PO_3^-] - 5k_4[H^+]^5[H_2PO_2^-] + 6k_6[Ni^{2+}]^3[PH_3]^2 \quad [18]$$

where $[\cdots]$ indicates a concentration of a chemical material in electrolyte. We set the concentrations of the following chemical species at the steady state to be $[H_3PO_3^-]_0 = x$, $[H_2PO_2^-]_0 = y$, $[PH_3]_0 = z$, $[H^+]_0 = s$, $[P]_0 = u$, and $[Ni^{2+}]_0 = v$. The concentrations of $H_2PO_3^-$, $H_2PO_2^-$, and Ni^{2+} in this study are so large that perturbed terms related to them can be ignored. Let Δz, Δu, and Δs denote the concentrations of $[PH_3]$, [P], and $[H^+]$ in the perturbed state, respectively. The linearized perturbation equations can be derived from Eq. 16-18

$$\Delta\dot{z} = 5k_4ys^4\Delta s - (4k_5zv^3 + k_7)\Delta z + k_6\Delta u \quad [19]$$

$$\Delta\dot{u} = 4k_5v^3z\Delta s - k_6\Delta u \quad [20]$$

$$\Delta\dot{s} = -(4k_2s + 4k_3sx + 25k_4s^4y)\Delta s + 12k_5v^3\Delta z \quad [21]$$

where $\Delta\dot{z} = dz/dt$. Instead of solving an eigenvalue problem of a 3×3 matrix for Eq. 19-21, for simplicity, we attempt to derive a second-order differential equation that describes an oscillatory behavior of the chemical reactions. The sum of Eq. 19 and 20 gives

$$\Delta\dot{z} + \Delta\dot{u} = 5k_4ys^4\Delta s - k_7\Delta z \quad [22]$$

Differentiating Eq. 16 and 18 with respect to t and using Eq. 19, we have

$$\Delta\ddot{z} + k_6\Delta\dot{z} + k_6k_7\Delta z = \text{const} \quad [23]$$

Hence, a condition for the oscillatory reactions is

$$k_6/k_7 < 4 \quad [24]$$

This condition only gives one upper limit of the reaction rate ratio. It is unclear at present whether or not the condition is valid because the experimental values of the two reaction rates are unknown. We cannot succeed in observing the oscillatory cell voltage with a fundamental frequency.[12,13] However, as the presence of the fundamen-

tal frequency f_0 is shown, we believe that there some oscillatory electrochemical reactions exist.

Conclusion

The ion species arriving at the cathode electrodes obeys the Poisson distribution by the measured scaling exponent $\alpha\beta = 1.05$. In addition, the exponent $v = 0.9$ and the fractal dimension 1.89 suggest that in Ni-P electrodeposition local effects such as shadowing can be negligible, and the ions arriving at the cathode can diffuse, in contrast to the DLA model. The power spectrum of the Fourier transformed cross-sectional Ni-P electrodeposit images reveals the presence of the fundamental frequency at which the number of the deposited particles vibrates. The interpretation of the oscillatory behaviors in the process is given by the solution of the electrochemical rate equations in the Ni-P-H system using the linearized perturbation equations.

Acknowledgment

M.S. thanks Hideki Higa at the University of the Ryukyus for his help and preparation of the experimental apparatus.

The University of the Ryukyus assisted in meeting the publication costs of this article.

References

1. J. Los, P. H. van Dam, W. J. P. van Enckevort, F. A. Hollande, and C. N. M. Keulemans, *J. Phys.: Condens. Matter,* **12**, 3195 (2000).
2. T. A. Witten and L. M. Sander, *Phys. Rev. B,* **27**, 5686 (1987).
3. M. Matsushita, Y. Hayakawa, and Y. Sawada, *Phys. Rev. A,* **32**, 3814 (1985).
4. C. A. Marozzi and A. C. Chialvo, *Electrochim. Acta,* **45**, 2111 (2000).
5. J. E. Williams and C. Davison, *J. Electrochem. Soc.*, **137**, 3260 (1990).
6. M. Saitou, Y. Okudaira, and W. Oshikawa, *J. Electrochem. Soc.*, **150**, C140 (2003).
7. T. M. Harriss and Q. D. Dang, *J. Electrochem. Soc.*, **140**, 81 (1993).
8. S. Karlin and H. M. Taylor, *A First Course in Stochastic Processes*, Academic Press, San Diego, CA (1975).
9. P. Meakin, *Phys. Rev. A,* **27**, 2616 (1983).
10. *CRC Handbook of Chemistry and Physics*, 79th ed., R. Linde, Editor, CRC Press, New York (1998).
11. E. J. Lowe, *Mellor's Comprehensive Treatise on Inorganic and Theoretical Chemistry*, Vol. 8, Suppl. 3, Longman, White Plains, NY (1971).
12. G. G. Láng, K. Ueno, M. Ujvári, and M. Seo, *J. Phys. Chem. B,* **104**, 2785 (2000).
13. A. Chen and B. Miller, *J. Phys. Chem. B,* **108**, 2245 (2004).